CrossMark

Microstructure and Corrosion Resistance of the AlTiN Coating Deposited by Arc Ion Plating

Qi-Xiang Fan[1] · Tie-Gang Wang[1] · Yan-Mei Liu[1] · Zheng-Huan Wu[1] · Tao Zhang[2] · Tong Li[3] · Zu-Bing Yang[1]

Abstract A new type of AlTiN coating containing about 29.13 at.% Al,16.02 at.% Ti and 54.85 at.% N was prepared by arc ion plating technology. The coating is composed of singular fcc-(Al, Ti)N phase and has no hcp-AlN phase to be formed. Due to the high content of beneficial element Al, the hardness and effective elastic modulus of the coating are up to 33.9 and 486.1 GPa, respectively. The adhesion strength between the coating and substrate is about 39.7 N. Electrochemical test shows that the corrosion current density of the AlTiN coating is nearly one-sixth of the substrate, and the charge transfer resistance R_{ct} of the AlTiN coating is much larger than that of the substrate, which means that the coating could act as a protective barrier between the substrate and corrosive electrolyte, enhancing the corrosion resistance.

KEY WORDS: Arc ion plating; AlTiN coating; Corrosion behavior; Microstructure; Hardness

1 Introduction

Nitride coatings mainly based on titanium, aluminum and chromium have been widely used as protective hard coatings in various harsh working environments owing to their high hardness and wear resistance, good thermal stability and corrosion resistance, low friction coefficient and superior chemical inertness, etc. [1]. TiN commercialized in the early

✉ Qi-Xiang Fan
  qxfan2015@163.com

✉ Tie-Gang Wang
  tgwang@tute.edu.cn

1 Tianjin Key Laboratory of High Speed Cutting and Precision Machining, Tianjin University of Technology and Education, Tianjin 300222, China

2 Division of State-owned Assets Management, Tianjin University of Technology and Education, Tianjin 300222, China

3 College of Electronic Engineering, Tianjin University of Technology and Education, Tianjin 300222, China

1980s is the first generation of physical vapor deposition (PVD) hard coating and is still widely used in cutting tools, dies as well as many mechanical components due to its high hardness and good wear resistance [2–5]. The oxidation resistance of TiN coating is poor since it would be oxidized quickly at the temperature above 500 °C forming a brittle and loose layer of TiO_2 [6]. Compared with the TiN coatings, the $Ti_{1-x}Al_xN$ coatings possess improved corrosion resistance, oxidation resistance and thermal stability, since a dense mixed-oxide film of Al_2O_3 and TiO_2 would form on the coating surface under corrosive environments or at elevated temperature which could act as a barrier hindering the diffusion of corrosive medium like O_2 into the interior coating and thus improve the oxidation resistance [7, 8]. The $Ti_{1-x}Al_xN$ coatings possess face-centered cubic (fcc) structure with Al atoms substituting for the Ti atoms [7]. Because the atom radius of Al is smaller than that of Ti, the lattice constant of $Ti_{1-x}Al_xN$ coatings is smaller than that of TiN coatings, and the hardness is higher. It was reported that the oxidation resistance and hardness of the nitride coatings were improved with increasing Al content [9, 10]. Consequently, the AlTiN coatings with x more than 0.5 are one of the promising coatings for near-dry or dry high-speed

cutting operations [11, 12]. However, AlN with wurtzite structure (hardness 12 GPa) would be formed with Al content exceeding the maximum solubility ($x = $Al/$(Al + Ti) = 0.65$–$0.75$) in the cubic phase [13, 14], leading to a decrease in hardness, bulk elastic, shear moduli and wear resistance. Thus, the synthesis of single cubic AlTiN coating with high Al content is a challenging task.

Feng et al. [15] and Xu et al. [16] prepared cubic $Al_{0.64}Ti_{0.36}N$ coatings by cathodic arc evaporation, since the high deposition rate could increase the solubility of Al. Their researches showed that the $Al_{0.64}Ti_{0.36}N$ coatings possessed good mechanical properties and oxidation resistance. Some other researchers applied multilayer architecture to increase the solubility limitation of Al in the cubic Ti–Al–N system by controlling the coherent growth. Todt et al. [17] prepared a kind of Al-rich cubic $Al_{0.8}Ti_{0.2}N$ coating with nano-lamellar microstructure by low-pressure chemical vapor deposition (PLCVD). Chen et al. [18] deposited a $Al_{0.66}Ti_{0.34}N/Ti_{0.52}Al_{0.48}N$ multilayer coating with cubic structure by cathodic arc evaporation. These multilayer coatings exhibit high hardness and good oxidation resistance because of the high Al content. Compared with single-layer coating, the preparation process of multilayer coating is difficult, and the modulation period must be very small to avoid the formation of h-AlN completely.

Hard coatings can be obtained by chemical vapor deposition (CVD) or PVD techniques such as thermal spray, ion-beam deposition, arc ion deposition and magnetron sputtering [19]. Among them, arc ion plating is one of the most widely used technologies owing to its high deposition rate and high energy of ions [16]. The coatings deposited by arc ion plating possess high density and strong adhesion. However, the macro defects such as inclusion and voids formed due to the micrometal droplets emitted from the cathodes reduce the corrosion resistance of the coatings. In many application, the coated parts are frequently exposed to an aggressive working environment, for instance, a Cl^--containing corrosive medium, particularly in a marine region, due to the strong effect of Cl^- in promoting localized corrosion [2]. Thus, it is important to study the corrosion resistance of the coatings before they are applied into industry. In this paper, a new type of $Al_xTi_{1-x}N$ coating with x of ~ 0.65 is developed by arc ion plating technology. The microstructure, mechanical properties and corrosion resistance of the coating were investigated in detail.

2 Experimental

2.1 Deposition of AlTiN Coating

The AlTiN coating was deposited on a piece of high-speed steel (HSS) by arc ion plating. The substrate with diameter

of 2 cm was ground down to 2000 # SiC paper and then mirror-polished to $Ra < 0.05$ μm. After ultrasonically cleaned within acetone, ethanol and deionized water successively, the substrate was dried and fixed onto the rotating substrate holder at a distance of 120 mm from the target in the vacuum chamber. To improve the uniformity of the film, the substrate holder was rotated at a speed of 10 r/min. The chamber was evacuated to at least 5×10^{-4} Pa by two mechanical pumps as well as one molecular pump, and then the substrate was heated to 400 °C. The elemental Ti and Al with purity of 99.99% were used as the targets. Prior to the deposition of AlTiN coating, the substrate was cleaned by Ar ion bombardment under -700 V negative bias voltage for 10 min, which would remove contaminants and enhance the adhesion strength between the film and the substrate. The current of Ti target was 50–100 A. After that, the bias voltage decreased to 60 V to deposit a Ti interlayer. This process lasted for about 10 min. Then N_2 was provided, and the Al target was powered on. The detail deposition parameters for the AlTiN coating prepared by arc ion plating technique are listed in Table 1.

2.2 Characterization

Phase identifications of the AlTiN coating were carried out using the glancing X-ray diffraction (XRD, X′ Pert PRD, PANalytical, Holland) to minimize the effect of high peak intensity of the high-speed steel. Surface and cross-sectional morphologies of the coating were observed under a scanning electron microscope (SEM, Inspect F) equipment with an electron-dispersive X-ray spectrometer (EDS) for compositional analysis. The surface roughness of the coating was measured by using a surface profiler (Alpha-Step IQ, KLA Tencor).

The mechanical properties of the AlTiN coating were measured by using a nano-indentation tester (Nano

Table 1 Deposition parameters of the AlTiN coating by arc ion plating technology

Parameters	Value
Base pressure (Pa)	5×10^{-4}
Working pressure (Pa)	2
Bias voltage (V)	-60
Ar flow (sccm)	50–100
N_2 flow (sccm)	300–400
Deposition temperature (°C)	400
Deposition time (min)	90
Arc current of Ti target (A)	50–100
Arc current of Al target (A)	50–100
Distance between the substrate and target (mm)	120

indenter G200, Agilent Technologies, USA) with a Ber-kovich indenter tip under the continuous stiffness mode. Ten separated measurements were taken on the AlTiN coating to obtain the average value. The distance between each indentations was at least 30 times of the maximum depth of indentation to prevent stress field effects from nearby indentations. The maximum depth of indentation was set as 1500 nm. The calibration of the film hardness values was checked by measuring on a standard sample (fused silica). The hardness and elastic modulus of the sample were 8.86 ± 0.11 and 72.1 ± 0.3 GPa, respectively. To avoid the effect of the substrate and get hardness (H) as well as effective elastic modulus (E^*) more accurately, the measured values are chosen at the indentation depth less than 10% of the film thickness. Here, E^* is given directly by the nano-indentation tester based on the formula $E^* = E/(1 - \upsilon^2)$, where E is the elastic modulus and υ is the Poisson's ratio.

The adhesion strength between the coating and substrate was measured by a scratch tester (J&L Tech, Scratch test JLST022) with a Rockwell C diamond stylus (cone apex angle: 120°; tip radius: 200 μm) that was moved across the sample surface. During the scratch tests, the normal load was increased from 0 to 100 N with a loading rate of 1 N/s and a translation speed of 0.2 mm/s. The friction force, friction coefficient, and acoustic emission signals were also recorded during the scratch tests in order to measure the critical load. The scratch tracks were observed under an optical microscope (OM, Olympus PMG3-613U W/Acc).

The electrochemical measurements of the AlTiN coating were taken in a 3.5 wt% NaCl solution, since chloride ion-containing environments are very common. The electrochemical properties of the AlTiN coating were tested by Gamry Instruments (USA) with an active area of 1 cm². A three-electrode system was used, consisting of a saturated calomel electrode (SCE) as a reference, a pure platinum sheet as counter electrode and the coated sample under test as the working electrode. The electrolyte employed was 3.5 wt% sodium chloride solution, prepared with analytical grease reagents and deionized water. Before the electrochemical measurements, samples were allowed to stabilize at their open-circuit potential (E_{oc}) for 30 min. The potentiodynamic polarization measurements were taken starting from −200 mV cathodically with respect to the open-circuit potential at a constant scan rate of 0.5 mV/s. The electrochemical impedance spectroscopy (EIS) measurement was taken using a scanning frequency ranging from 10^{-2} to 10^5 Hz, and the testing signal is 20 mV. All the measurements are taken at room temperature (22 °C). Based on an appropriate electrical equivalent circuit, the Nyquist plots obtained from the EIS measurements were fitted by ZSimpwin 3.20 software to calculate the corresponding parameters.

3 Results and Discussion

3.1 Microstructure Characterization

Figure 1 shows the XRD patterns of the AlTiN coating deposited by arc ion plating. As can be seen, the coating exhibits a single fcc structure with multiple orientations of (111), (200), (220), (311) and (222) crystal planes. The diffraction peaks lie between those of fcc TiN (PDF# 25-1495) and AlN (PDF# 38-1420) phases, indicating that the fcc (Al, Ti)N solid solution phase forms, while the B4-wurtzite AlN (PDF# 25-133) does not form. The AlTiN coating contains higher Al content than Ti content; therefore, the diffraction peaks of the coating are closer to those of AlN which possesses smaller lattice constant than TiN. The preferred orientation of the AlTiN coating is (111) crystal plane which has the lowest surface energy in the fcc structure [20]. The preferred orientation is usually the crystal plane which possesses the minimum overall energy between surface energy and strain energy during the deposition process [21, 22]. Since the strain energy of (200) plane is smaller than that of the (111) plane [23], the preferred orientation would be (200) crystal plane when the deposition parameters such as deposition temperature and bias voltage change [4, 24].

Figure 2 shows the surface morphologies of the AlTiN coating deposited by arc ion plating. As shown in Fig. 2, there are some white particles and pinholes on the dark gray surface. The white particles are macro-particles resulting from the droplets which were emitted from the arc spots in the Al target or Ti target and solidified before they arrived at the substrate. The macro-particles shrink at the ambient temperature after deposition. The macro-particles possess larger specific area than the coating around them,
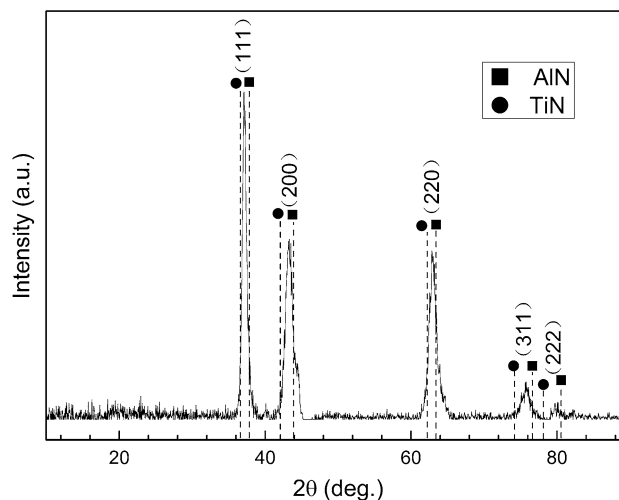

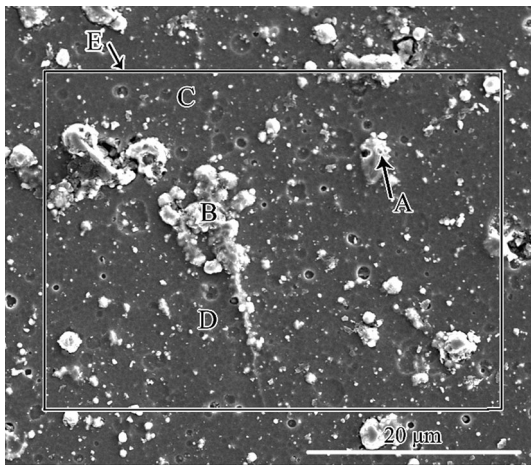**Fig. 1** XRD patterns of the AlTiN coating deposited by arc ion plating technology

Fig. 2 Surface morphologies of the AlTiN coating deposited by arc ion plating technology

Fig. 3 Cross-sectional morphology of the AlTiN coating deposited by arc ion plating technology

Table 2 Elemental compositions of four different points (A, B, C, D) and one selected area (E) on the surface of the AlTiN coating

Position	Al (at.%)	Ti (at.%)	N (at.%)	Al/(Al + Ti) (x)
A	28.35	15.37	56.26	0.648
B	25.20	15.13	59.68	0.625
C	32.71	18.87	48.42	0.634
D	29.80	15.04	55.16	0.665
E	29.13	16.02	54.85	0.645

thereby they shrink more obviously, and some might flake from the surface resulting in the pits and pinholes left on the coatings [25, 26]. Because of these macro-particles and pinholes, the surface roughness of the coating is high (about 214.3 nm) measured by surface profiler.

The elemental compositions at four different points (A, B, C, D in Fig. 2) and in one selected area (inside area of the rectangle E in Fig. 2) on the surface of the AlTiN coating are analyzed by EDS, which is listed in Table 2. As can be seen, the white macro-particles contain more N element than the dark gray spots, and the Al/(Al + Ti) values range from 0.625 to 0.665. The elemental compositions in the rectangle E is about 29.13 at.% Al, 16.02 at.% Ti and 54.85 at.% N. The Al/(Al + Ti) value is about 0.65. Since the selected area E includes the four points (A, B, C, D), the elemental compositions of this area E are taken as the average elemental compositions of the coating. The cross-sectional morphology of the AlTiN coating is presented in Fig. 3. It can be seen that a very thin layer of Ti lies between the AlTiN coating and the substrate, which plays an important role in the improvement of adhesive strength. The AlTiN coating is dense, and the thickness is about 3.0 μm.
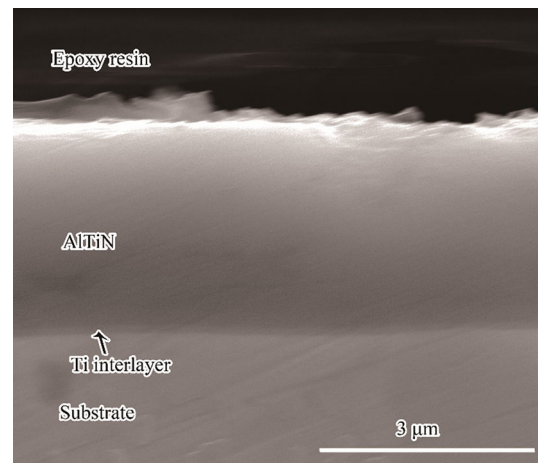
3.2 Mechanical Properties

The hardness versus displacement and modulus versus displacement curves of the AlTiN coating are presented in Fig. 4. These two curves show the same trend which could be divided into three stages: quickly increasing stage, plateau stage and declining stage. The average hardness value at the plateau stage could be considered as the real hardness of the films. Note that the indentation depth at this region is less than 10% of the film thickness, which could be deemed to minimize the effect of the substrate greatly. The hardness and effective modulus (E^*) of the AlTiN coating are about 33.94 and 486.1 GPa, respectively. The high hardness of the coating is attributed to the solid solution hardening of the element Al which decreases the lattice constant of the coating. It is consistent with the XRD pattern (Fig. 1) that the diffraction peaks of the AlTiN coating shift to higher angles, compared with those of TiN phase.

The adhesion strength of the AlTiN coating was measured by scratching its surface with the normal load increasing gradually from 0 to 100 N. During the process, plastic deformation occurs at the beginning; then, some cracks form and flakes might be generated along the track subsequently. Finally, large spallation outside the track happens and makes the coating detach from the substrate indicating the total failure of the film [27]. Figure 5 shows the morphology of the scratch track of the AlTiN coating. When the normal force is up to about 39.7 N, large spallation occurs and the coating is removed from the substrate. The adhesion strength of a coating/substrate system is normally defined as the energy to separate a coating from the substrate [28]. Thus, the adhesion strength of the AlTiN coating is about 39.7 N.
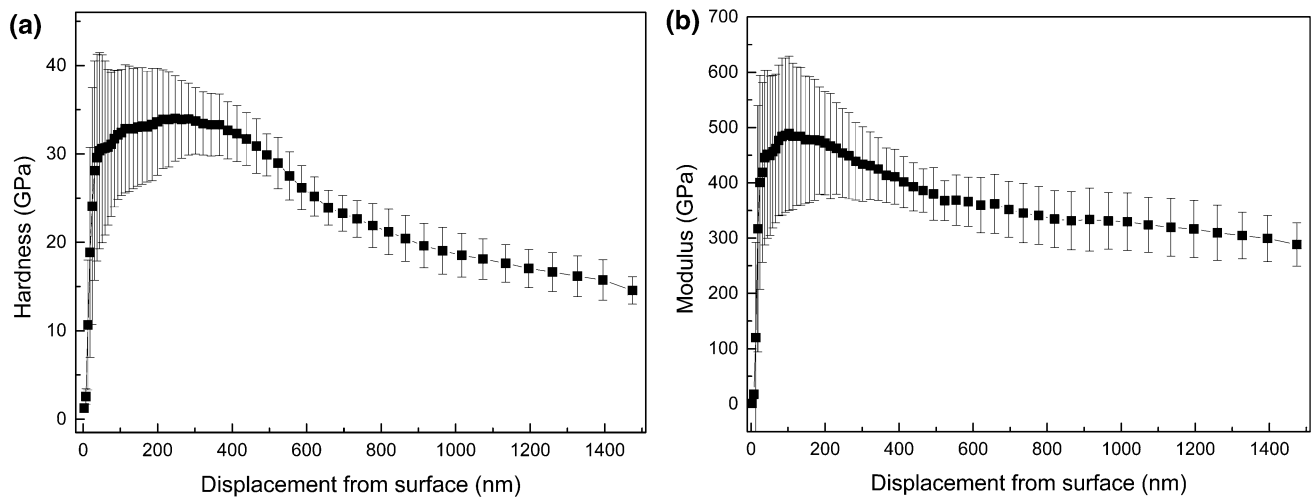
(a)

(b)

Fig. 4 Hardness versus displacement **a** and modulus versus displacement and **b** of the AlTiN coating measured by nano-indenter tester
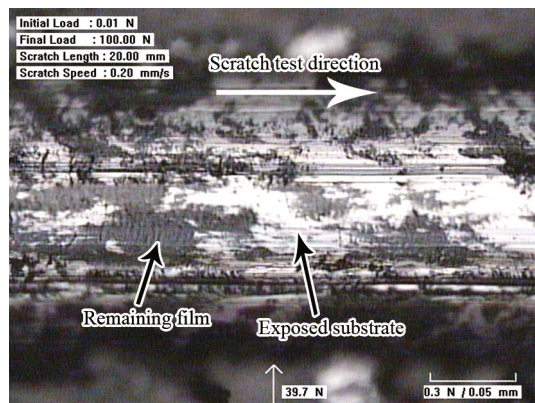

Fig. 5 Morphology of scratch track of the AlTiN coating observed by optical microscopy

3.3 Electrochemical Properties

The potentiodynamic polarization curves of the substrate and AlTiN coating in a 3.5 wt% NaCl solution are shown in Fig. 6. The corrosion potential E_{corr} and current density I_{corr} of the substrate are about -0.5019 V and 11.392 $\mu A/cm^2$, respectively, while for the AlTiN coating the corrosion potential is -0.4999 V and the current density is 1.861 $\mu A/cm^2$ according to the Tafel extrapolation method. The potential of AlTiN coating is slightly lower than that of the substrate, owing to the high electrochemical activity of Al and Ti. However, the corrosion current density of the AlTiN coating is nearly one-sixth of that of the substrate. The value of the corrosion potential reflects the corrosion tendency of the materials in thermodynamics, and the value of the corrosion current density reflects the corrosion rate of the material in kinetics [29]. Usually, I_{corr} is cited as a criterion to evaluate the kinetics of a corrosion process, and
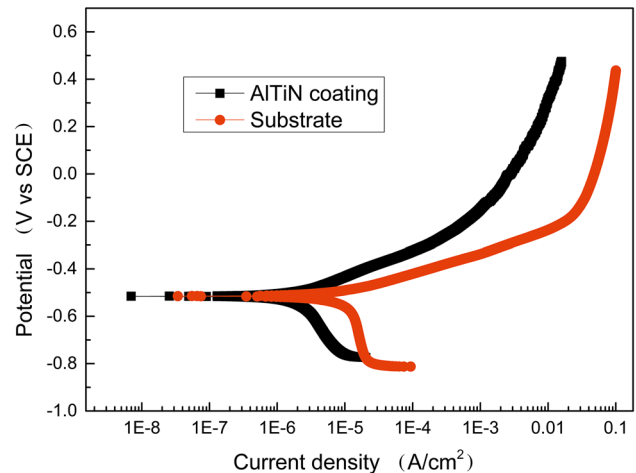

Fig. 6 Potentiodynamic polarization curves of the substrate and AlTiN coating in 3.5 wt% NaCl solution

it is normally proportional to the corrosion rate [1]. The corrosion current density of the AlTiN coating is lower than that of the substrate meaning that it possesses better corrosion resistance than the substrate. The nitride coatings could form thin passive oxide layers on the coatings' surface when the coating samples are contacting with the NaCl solution [2]. Since the AlTiN coating contains high Al content about 30.58 at.%, and the Gibbs free energy of Al_2O_3 is lower than that of TiO_2, a continuous and dense oxide layer mainly composed of alumina could be formed on the surface of the coating during the corrosion process [30, 31]. The oxide layer can act as a protective barrier between the substrate and the corrosive electrolyte, enhancing the corrosion resistance greatly.

The EIS of the substrate and AlTiN coating in 3.5 wt% NaCl solution is illustrated in Fig. 7. The EIS of the
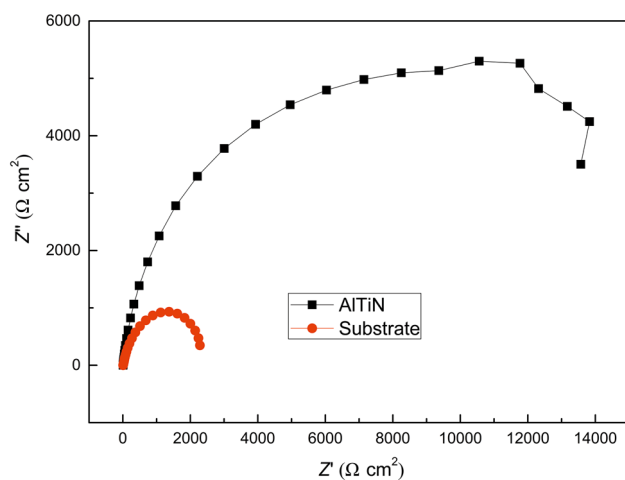
Fig. 7 Electrochemical impedance spectroscopy (EIS) of the substrate and AlTiN coating in 3.5 wt% NaCl solution
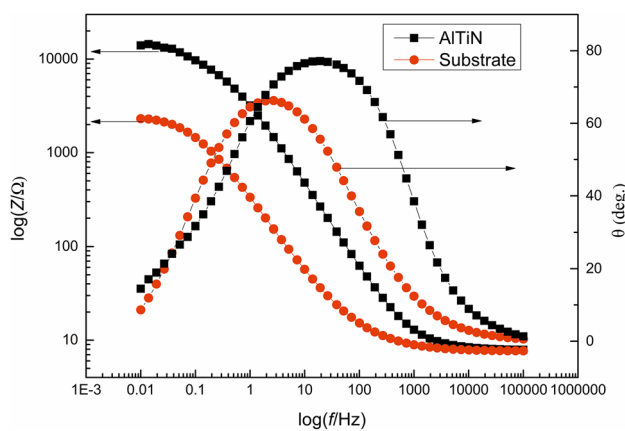

Fig. 8 Bode and phase diagram of the substrate and AlTiN coating in 3.5 wt% NaCl solution

Fig. 9 Equivalent electrical circuit for the EIS data of the substrate **a** and AlTiN coating **b** corroded in 3.5 wt% NaCl solution

substrate and the AlTiN coating shows an irregular semicircle indicating a single time constant, for the samples were exposed in the corrosive medium for just approximately 1 h, which is not sufficient to reveal the degradation of the substrate. Usually, the larger the diameter of the capacitive loop, the better the corrosion resistance of the sample [32]. The AlTiN coating possesses a larger capacitive resistance than the substrate, indicating that the AlTiN coating has better corrosion resistance. As shown in Fig. 8, the absolute impedance of the AlTiN coating is much larger than that of the substrate, which also indicates that the AlTiN coating possesses superior corrosion resistance to the substrate.

After ZsimpWin 3.20 software fitting, the EIS data of the substrate and AlTiN coating can be fit well with the equivalent circuit in Fig. 9a, b, respectively. In the equivalent circuit, the electrolyte resistance R_{s} is electrolyte solution resistance between the working electrode and the
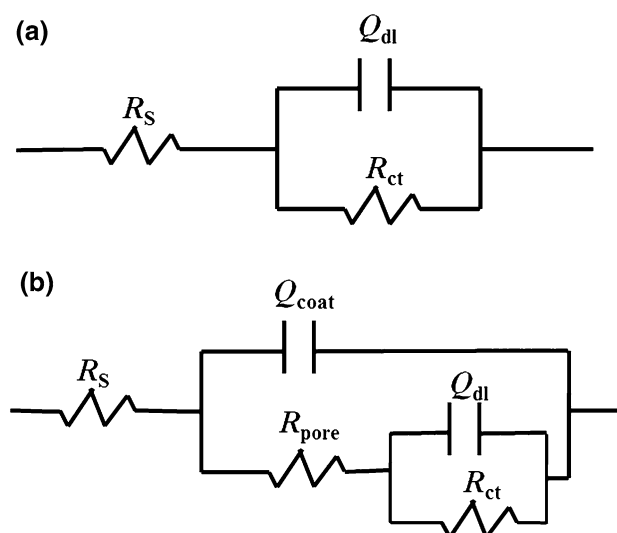
reference electrode. Q_{dl} is a double-layer capacitance related to the electrochemical process occurring between the alloy and the solution, while R_{ct} represents the charge transfer process happening between the alloy and the electrolyte. For the AlTiN coating, the equivalent circuit contains two additional elements, the capacitance Q_{coat} and the charge transfer resistance R_{pore} resulting from the formation of ionic conduction path across the coating. The corrosion interface is characterized by a parallel capacitor with a double-layer constant phase element Q_{dl} and charge transfer resistance R_{ct}. Note that Q stands for constant phase element, which is responsible for deviation from ideal dielectric behavior of a non-ideal capacitor. The admittance is given by:

$$Y(\omega) = Y_{0}(j\omega)^{n}, \tag{1}$$

where Y_{0} is the adjustable parameter used in the nonlinear least squares fitting, j is $\sqrt{-1}$, ω is the angular frequency, and n is also an adjustable parameter which always lies in -1 and 1. For $n = 1$, Y represents a capacitance, while for $n < 1$, Q is a non-ideal capacitor. For $n = -1$, Y represents an inductance; for $n = 0$, Y represents a resistance.

The parameters extracted from the EIS data of the bare alloy and AlTiN coating corroded in 3.5 wt% NaCl solution is presented in Table 3. The charge transfer resistance R_{ct} of the AlTiN coating is about 1.22×10^{4} Ω cm^{2}, which is much larger than that of the substrate (2633 Ω cm^{2}). Usually, the higher the charge transfer resistance, the better the corrosion resistance of the material [33]. In addition, the double-layer capacitance of the AlTiN coating is 2.93×10^{-4} μF/cm^{2}, smaller than that of the substrate (6.358×10^{-4} μF/cm^{2}), which indicates that the number of electric charge and ion at the corrosive interface is less,

Table 3 Parameters extracted from the EIS data of the substrate and AlTiN coating corroded in 3.5 wt% NaCl solution

Sample	R_s (Ω cm^2)	$Q_{coat} - Y_o$ (μF/cm^2)	n_c	R_{pore} (Ω cm^2)	$Q_{dl} - Y_o$ (μF/cm^2)	n_{dl}	R_{ct} (Ω cm^2)
Substrate	8.046	–	–	–	6.358×10^{-4}	0.7779	2633
AlTiN	8.68	5.43×10^{-5}	0.8833	8536	2.93×10^{-4}	0.612	1.22×10^4

revealing that the AlTiN film is corroded milder than the bare alloy. It is consistent with the potentiodynamic polarization result. Thus, it can be concluded that the coating can act as a protective barrier between the substrate and the corrosive electrolyte and enhance corrosion resistance effectively regardless of the presence of macro-particles and pinholes on the surface.

3.4 Porosity of Coating

The porosity of a coating has a great impact on the properties of the coating. If the coatings possess high porosity, severe corrosion between the coating and substrate would occur, since the substrate would take as the anode. Several electrochemical methods could estimate the porosity of a coating [34]. For nitride coatings, the porosity of a coating can be determined from the polarization resistance measurements according to Eq. (2) [1, 34]:

$$P = \left(\frac{R_{ps}}{R_p}\right) \times 10^{-|\Delta E_{corr}|/\beta_a}, \tag{2}$$

where, P is the total coating porosity; R_{ps} and R_p are the polarization resistance of the substrate and the coating, respectively; ΔE_{corr} is the difference between the corrosion potential of the coating and the substrate; β_a is the anodic Tafel slope of the substrate.

According to Table 3, R_{ps} is equal to 2633 Ω cm^2, and R_p is 2.0556×10^4 Ω cm^2 (the combination of R_{pore} and R_{ct}). ΔE_{corr} is about 0.002 V, and β_a is 0.1074 V/decade by linear fitting the anode polarization curve. Putting these parameters in formula (2), the porosity can be calculated out as 12.27%.

4 Conclusions

1. A new type of AlTiN coating with Al/(Al + Ti) about 0.65 was prepared on a high-speed steel by arc ion plating technology. The coating consists of singular fcc-(Al, Ti)N phase with preferred orientation (111) crystal plane.
2. The hardness and the elastic modulus of the AlTiN coating are about 33.94 and 486.1 GPa, respectively. The adhesion strength between the coating and substrate is 39.7 N.

3. The AlTiN coating possesses lower corrosion current density and larger charge transfer resistance than the bare alloy, which indicates that the coating has better corrosion resistance in 3.5 wt% NaCl electrolyte and could act as a protective barrier between the substrate and corrosive electrolyte.

References

[1] L. Zhang, Y. Chen, Y. Feng, S. Chen, Q. Wan, J. Zhu, Int. J. Refract. Metals Hard Mater. **53**, 68 (2015)
[2] X.Z. Ding, A.L.K. Tan, X.T. Zeng, C. Wang, T. Yue, C.Q. Sun, Thin Solid Films **516**, 5716 (2008)
[3] Z. Wang, D. Zhang, P. Ke, X. Liu, A. Wang, J. Mater. Sci. Technol. **31**, 37 (2015)
[4] Y.H. Zhao, W.J. Yang, C.Q. Guo, Y.Q. Chen, B.H. Yu, J.Q. Xiao, Acta Metall. Sin. (Engl. Lett.) **28**, 10 (2015)
[5] X. Chen, J. Zhang, S. Ma, H. Hu, Z. Zhou, Acta Metall. Sin. (Engl. Lett.) **27**, 31 (2014)
[6] D. McIntyre, J. Greene, G. Håkansson, J.E. Sundgren, W.D. Münz, J. Appl. Phys. **67**, 1542 (1990)
[7] D. Kong, H. Guo, Tribol. Int. **88**, 31 (2015)
[8] D. Kong, G. Fu, J. Mater. Res. **30**, 503 (2015)
[9] J. Peng, D. Su, C. Wang, J. Mater. Sci. Technol. **30**, 803 (2014)
[10] T. Polcar, A. Cavaleiro, Mater. Chem. Phys. **129**, 195 (2011)
[11] M.I. Yousaf, V.O. Pelenovich, B. Yang, C.S. Liu, D.J. Fu, Surf. Coat. Technol. **265**, 117 (2015)
[12] X. Wang, P.Y. Kwon, D. Schrock, D. Kim, Wear **304**, 67 (2013)
[13] L. Chen, M. Moser, Y. Du, P.H. Mayrhofer, Thin Solid Films **517**, 6635 (2009)
[14] Y. Makino, K. Nogi, Surf. Coat. Technol. **98**, 1008 (1998)
[15] Y. Feng, L. Zhang, R. Ke, Q. Wan, Z. Wang, Z. Lu, Int. J. Refract. Metals Hard Mater. **43**, 241 (2014)
[16] Y. Xu, K. Chen, S. Wang, C. Pan, S. Chen, Vacuum **131**, 97 (2016)
[17] J. Todt, J. Zalesal, R. Daniel, R. Pitonak, A. Köpf, R. Weißenbacher, B. Sartory, C. Mitterer, J. Keckes, Surf. Coat. Technol. **291**, 89 (2016)
[18] L. Chen, Y. Xu, Y. Du, Y. Liu, Thin Solid Films **592**, 207 (2015)
[19] V.K.W. Grips, H.C. Barshilia, V.E. Selvi, Kalavati, K.S. Rajam, Thin Solid Films **514**, 204 (2006)
[20] H. Jiménez, E. Restrepo, A. Devia, Surf. Coat. Technol. **201**, 1594 (2006)

[21] P.J. Martin, A. Bendavid, T.J. Kinder, I.E.E.E. Trans, Plasma Sci. **25**, 264 (1997)

[22] G.Q. Yu, B.K. Tay, S.P. Lau, K. Prasad, L.K. Pan, J.W. Chai, D. Lai, Chem. Phys. Lett. **374**, 264 (2003)

[23] J. Pelleg, L.Z. Zevin, S. Lungo, N. Croitoru, Thin Solid Films **197**, 117 (1991)

[24] F. Cai, S. Zhang, J. Li, Z. Chen, M. Li, L. Wang, Appl. Surf. Sci. **258**, 1819 (2011)

[25] C.M. Shi, T.G. Wang, Z.L. Pei, J. Gong, C. Sun, J. Mater. Sci. Technol. **30**, 1193 (2014)

[26] T.G. Wang, D. Jeong, S.H. Kim, Q. Wang, D.W. Shin, S. Melin, S. Iyengar, K.H. Kim, Surf. Coat. Technol. **206**, 2629 (2012)

[27] Y.M. Liu, C.L. Jiang, Z.L. Pei, H. Lei, J. Gong, C. Sun, Surf. Coat. Technol. **245**, 108 (2014)

[28] T.G. Wang, D. Jeong, Y. Liu, Q. Wang, S. Iyengar, S. Melin, K.H. Kim, Surf. Coat. Technol. **206**, 2638 (2012)

[29] N. Perez, *Electrochemical and Corrosion Science* (Chemical Insustry Press, Beijing, 2013), p. 54. **(in Chinese)**

[30] Y.J. Liang (ed.), *Handbook of Thermodynamics Data for Inorganic Coumpounds* (Northeastern University Press, Shenyang, 1993)

[31] D.L. Wu, S.M. Jiang, Q.X. Fan, J. Gong, C. Sun, Acta Metall. Sin. (Engl. Lett.) **27**, 627 (2014)

[32] L.M. Chang, D. Chen, S.Y. Shi, Mater. Prot. **41**, 17 (2008). **(in Chinese)**

[33] Y. Li, L. Qu, F.H. Wang, Z.B. Shao, J. Chin. Soc. Corros. Prot. **23**, 65 (2003). **(in Chinese)**

[34] J. Creus, H. Mazille, H. Idrissi, Surf. Coat. Technol. **130**, 224 (2000)